Numerical analysis on seismic performance of small-sized earth dams with crest improvement using Newmark-D method

Shunichi Ohyama[1], *Akira* Izumi[1], and *Yutaka* Sawada[2*]

[1] Institute for Rural Engineering, National Agriculture and Food Research Organization, Tsukuba, Ibaraki, Japan
[2] Graduate School of Agricultural Science, Kobe University, Nada-ku, Kobe, Hyogo, Japan

Abstract. Small earth dams are widespread in Asia, and improving their seismic performance is critical for regional resilience. Crest improvement through cement stabilization can enhance apparent cohesion; however, the effect of partial crest improvement on overall seismic behavior remains uncertain. This study evaluated a 10-meter-high earth dam under infrequent but large-scale (Level-2) seismic motions to examine the applicability of the Newmark-D method to small-sized dams incorporating crest improvement and to assess how different improvement patterns influence seismic performance. Analytical results obtained from the Newmark-D method, which considers soil strength degradation during earthquakes, were compared with centrifuge test results. Findings show that shear strain concentrated near the interface between improved and unimproved zones, indicating potential shear failure and cracking. For cases without reinforcement and with crest improvement up to 15% of the embankment height, predicted crest settlement aligned well with experimental data when the maximum displacement arc passing through the crest was considered. In contrast, when the upper 30% of the embankment was reinforced, the analysis overestimated settlement compared to centrifuge test results, except in the A-type reinforcement geometry. This discrepancy likely arose because the Newmark-D method presumes slip along a failure surface, whereas no slip occurred in the centrifuge tests. In cases without sliding, advanced approaches such as elastoplastic finite-element modeling are recommended to obtain reliable results.

1 Background

Agriculture is highly dependent on water resources and represents the sector with the highest water consumption within industry [1]. In regions with limited water availability, numerous small earth dams have been constructed to secure agricultural water supplies. Japan has approximately 150,000 small earth dams, about 70% of which are more than 150 years old or have unknown construction dates [2]. Many of these small earth dams were built using empirical construction techniques and were neither designed nor constructed according to modern engineering standards.

Meanwhile, the Asian region experiences frequent earthquakes. In Japan, major earthquakes such as the Southern Hyogo Prefecture Earthquake, and the 2011 off the Pacific Coast of Tohoku Earthquake have occurred in the past, causing damage to many small earth dams, including embankment settlement, sliding, cracking, and even dam failures [3–5]. Therefore, it is essential to enhance the seismic performance of small earth dams and to implement appropriate measures to mitigate earthquake-induced damage.

Seismic retrofitting methods for small earth dams include counterweight fill, steel sheet pile installation, and reinforced embankment techniques [6–8]. Among these, the counterweight fill method is commonly used; however, it cannot be applied in cases where a reduction in storage capacity is unacceptable or where land-use constraints exist. Furthermore, the steel sheet pile method requires substantial temporary construction work and high material costs, making it difficult to apply widely to the large number of small earth dams across the country. Although the reinforced embankment method is a viable alternative, it also tends to be more costly than counterweight fill. Therefore, there is a need for seismic retrofitting methods for small earth dams that impose fewer construction constraints.

One seismic countermeasure capable of addressing these challenges involves adding solidifying agents, such as lime or cement-based stabilizers, to the embankment material to improve the strength of the crest. This method requires less excavation than full-scale retrofit or embankment reinforcement, thereby enabling more labor-efficient construction. Ohyama et al. [9] conducted centrifuge tests and demonstrated that crest improvement enhances the seismic performance of small-sized earth dams. However, evaluation cases based on numerical analysis are limited, with existing studies restricted to the analysis conducted by Tani et al. [10], which examined only partial improvement of the fill dam crest. Consequently, the influence of different crest improvement patterns on seismic performance remains insufficiently understood.

In seismic performance verification of small earth dams under Level-2 seismic motion (infrequent but

* Corresponding author: sawa@harbor.kobe-u.ac.jp

large-scale seismic motions), settlement of the embankment is evaluated using dynamic response analysis or plastic slip analysis. If the calculated settlement is less than the specified allowable settlement, the seismic performance is considered adequate [6]. LIQCA is a representative analysis code for dynamic effective stress analysis and is widely used for seismic performance evaluation of embankment structures, including earth dams [11, 12]. Although dynamic effective stress analysis offers a high capability for reproducing the seismic behavior of small earth dams, it requires detailed soil parameters and appropriate constitutive models. As a result, the quality of the results can be sensitive to the input parameters and modelling assumptions, underscoring the need for sufficient analytical expertise to ensure reliable evaluations.

In contrast, the Newmark method—widely recognized as a fundamental procedure for plastic sliding analysis—constitutes a simplified framework that idealizes the sliding mass as a rigid body and represents the shear behavior along the potential failure surface using a quasi-plastic stress–strain relationship. Permanent seismic displacement is assessed by formulating the equation of motion based on the equilibrium between the inertial forces acting on the sliding mass and the shear resistance mobilized along the sliding surface. However, a major limitation of this classical method is its inability to account for strength degradation induced by liquefaction or cyclic loading during earthquakes. To address this limitation, the Newmark-D method has been proposed in recent years [13, 14]. This enhanced approach incorporates the progressive reduction in shear strength under undrained cyclic loading—represented through cumulative damage theory—into the conventional sliding displacement calculation, enabling a more mechanistically consistent evaluation of seismic deformation. The Newmark-D method has been regarded as a practical and physically grounded framework for assessing the seismic performance of small-sized earth dams subjected to prolonged Level-2 seismic motion, and its applicability has been demonstrated through its successful reproduction of the failure mechanism of the Fujinuma Dam, which breached during the 2011 off the Pacific Coast of Tohoku Earthquake [14, 15].

This study employs the Newmark-D method to assess the seismic performance of small-sized earth dam embankments incorporating crest improvement under Level-2 seismic motions. The objectives of this study were to examine the applicability of the Newmark-D method to small-scale earth dams with crest improvement and to evaluate how various crest improvement patterns influence the seismic performance.

2 Materials and methods

2.1 Overview of the analysis framework based on the Newmark-D method

The Newmark-D method is an analytical technique for evaluating seismic-induced slip deformation. This method extends the conventional Newmark sliding-block framework by incorporating the progressive degradation of soil strength under repeated undrained loading through cumulative damage theory. In doing so, it enables a more mechanistically consistent estimation of earthquake-induced slip displacement than that provided by the classical Newmark method. An overview of the analytical procedure adopted in this study is presented below. For a detailed description of the theoretical formulation and implementation of the Newmark-D method, readers are referred to Duttine et al. [13, 14].

First, a two-dimensional analytical model of the dam body and foundation ground is constructed, incorporating the stratigraphic configuration, material properties, water level, and input acceleration. Following an initial self-weight analysis, a dynamic response analysis (FEM-based analysis) is performed using, for example, an equivalent linearization approach that accounts for the strain-dependent variations in stiffness and damping. This analysis yields the initial stress state within the embankment, as well as the response accelerations and the corresponding time histories of stresses. Subsequently, the initial critical circular slip surface is identified, after which the shear strength τ_f at the base of each slice is computed using the following equation.

$$\tau_f = c + \sigma'\cdot\tan\phi = F_s\cdot s_{mi}/L_i \tag{1}$$

Here, F_s denotes the factor of safety against sliding, s_{mi} represents the mobilized shear force at the base of each slice, and L_i is the length of the base of each slice.

Under drained conditions, the effective strength parameters c' and ϕ' are used, whereas under saturated undrained conditions, the apparent cohesion c_u and internal friction angle ϕ_u obtained from total-stress testing are adopted as input parameters in Eq. 1. In saturated undrained conditions, soil strength decreases due to undrained cyclic loading, during which excess pore water pressure accumulates and reduces the effective stress. The variable σ' denotes the effective stress at the base of each slice. Under drained conditions, σ' is influenced by the horizontal seismic coefficient k_h, because changes in total stress are directly reflected in effective stress. Under saturated undrained conditions, excess pore pressure develops in response to seismic loading, counteracting the total stress increment. Consequently, σ' is considered unaffected by k_h and is taken as the initial effective stress σ_0'. Based on these definitions, the critical circular slip surface C_0, which yields the minimum yield seismic coefficient under a constant horizontal seismic coefficient k_h , is determined using the limit-equilibrium method (Fellenius method).

The time history of the effective shear stress τ_w acting at the base of each slice along the identified critical circular slip surface C_0 is decomposed into a sequence of stress pulses, and the double amplitude of shear strain (DA) is evaluated using cumulative damage theory. For each pulse i, the stress amplitude ratio SR,

$$SR = \Delta\tau / 2\sigma_0' \tag{2}$$

is determined, and the corresponding number of cycles N_i is obtained from the SR–log N_c relationship established through undrained cyclic triaxial tests. The damage index for each pulse is defined as

$$D_i = 1/N_i \tag{3}$$

When the cumulative damage $D = \sum D_i$ reaches unity, the associated DA is considered to have developed. The relationship between this DA and the shear strength τ_f is formulated based on the results of monotonic loading tests conducted after cyclic loading. Using this relationship, the time history of τ_f at the base of each slice is subsequently updated.

From the response accelerations obtained in the dynamic response analysis, the average acceleration of the sliding soil mass is evaluated. The time history of the rotational acceleration $\ddot{\theta}$ is then computed for those time intervals in which the driving moment M_d exceeds the resisting moment M_r (Eq. 5). By integrating the rotational acceleration $\ddot{\theta}$ twice with respect to time, the time history of the slip displacement

$$\delta = R \cdot \theta \tag{4}$$

is obtained. The resisting moment M_r and driving moment M_d are calculated using Eq. 6 and Eq. 7, respectively:

$$M \cdot (R_G)^2 \cdot \ddot{\theta} = M_d - M_r \tag{5}$$

$$M_r = \sum \{R \cdot (\tau_f \cdot L_i)\} \tag{6}$$

$$M_d = M \cdot g \cdot r + M \cdot R_G \cdot \ddot{x} \tag{7}$$

Here, M is the mass of the sliding soil block, g is the gravitational acceleration, r is the horizontal distance between the center of rotation and the center of gravity, R_G is the radius to the center of gravity of the sliding block, $\ddot{x}$ is the average response acceleration within the sliding block, R is the radius of the circular slip surface, τ_f is the shear strength at the base of each slice, and L_i is the base length of slice i.

This procedure is repeated iteratively to identify the critical circular slip surface that yields the maximum residual displacement.

2.2 Analysis conditions

The analysis considered the five cases illustrated in Fig. 1. CASE 1 represents the baseline condition without countermeasures. CASE 2 and CASE 3 correspond to configurations in which the crest of the dam was improved by 15% and 30%, respectively. CASE 4 and CASE 5 extend the CASE 3 configuration by further modifying the improved zone into A-type and T-type reinforcement geometries. All analyses were conducted following the procedure described in Section 2.1 and were based on the Newmark-D methodology. The initial stress analysis was performed using the Duncan–Chang constitutive model to account for the nonlinear behavior of the embankment materials, whereas the seismic response analysis was carried out using the equivalent linearization method. Subsequently, plastic sliding analysis was conducted employing the Newmark-D method. The analyses utilized SRA-X (Version 1.51) and SERID (Version 3.01), both developed by Godai Development Co., Ltd. The seepage line was established based on pore-water pressure measurements obtained from the centrifuge tests conducted by Ohyama et al. [9].

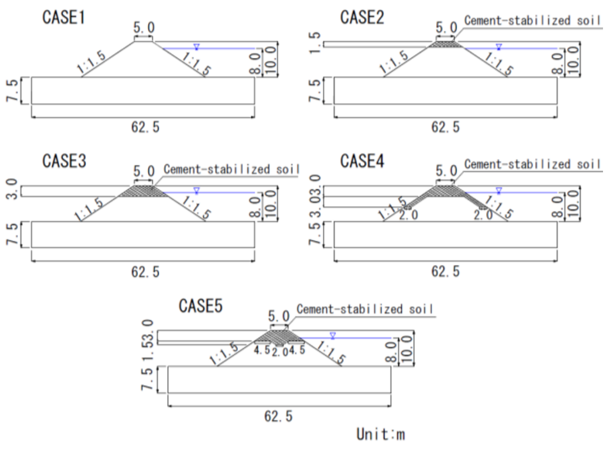

Fig. 1. Cross-section of the model embankment (CASE1—CASE5).

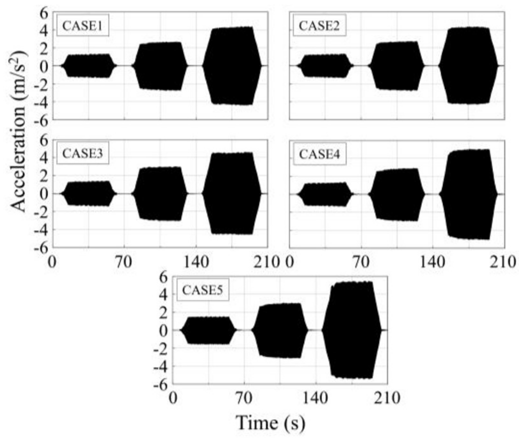

Fig. 2. Input acceleration for analysis in each case.

In the experiments, staged sinusoidal excitations with peak acceleration amplitudes of 1.5 m/s², 3.0 m/s², and 4.5 m/s² were applied. Each excitation stage had a constant frequency of 5 Hz and a duration of 60 s, including taper sections, corresponding to 300 loading cycles per stage. The same input acceleration employed in the shaking table during the centrifuge tests was used in the seismic response analysis. To account for the cumulative effects of the shaking history, the input acceleration from each excitation stage were concatenated into a single input motion. The input acceleration used for the seismic response analysis is presented in Fig. 2.

Because the SRA-X program used for the seismic response analysis does not incorporate stress-dependent shear modulus behavior, the embankment and foundation soils were discretized into 9–10 layers.

Table 1. Parameters used for initial stress analysis and parameters used for dynamic response analysis.

Category	γ_t (kN/m^3)	γ_{sat} (kN/m^3)	Duncan-Chang parameters										Material-specific parameters characteristic of the soil		Poisson's ratio
			K	n	R_f	c'	ϕ'	c_d	ϕ_d	G	F	D	A	n	v
Embankment and foundation	17.6	19.3	318.9	0.492	0.967	5.9	27.9	—	—	0.33	0	0	3767.5	0.492	0.49 (Saturated)
Cement-stabilized soil	17.6	19.3	685.5	0.540	0.850	—	—	13.3	34.5	0.33	0	0	4623.8	0.540	0.41 (Unsaturated)

Table 2. Parameters used for the plastic slip analysis.

	γ_t (kN/m^3)	γ_{sat} (kN/m^3)	Foundation and Embankment c' (kN/m^2) / ϕ' (°) (Unsat.)	Foundation and Embankment c (kN/m^2) / ϕ (°) (Sat.)	Cement-stabilized soil c_d (kN/m^2) / ϕ_d (°) (Unsat.)	Cement-stabilized soil c (kN/m^2) / ϕ (°) (Sat.)
CASE1	17.6	19.3	5.9 / 27.9	48.3 / 12.2	—	—
CASE2	17.6	19.3	5.9 / 27.9	48.3 / 12.2	13.3 / 34.5	—
CASE3	17.6	19.3	5.9 / 27.9	48.3 / 12.2	13.3 / 34.5	73.3 / 43.1
CASE4	17.6	19.3	5.9 / 27.9	48.3 / 12.2	13.3 / 34.5	73.3 / 43.1
CASE5	17.6	19.3	5.9 / 27.9	48.3 / 12.2	13.3 / 34.5	73.3 / 43.1

The initial shear modulus for each layer was computed using the average effective stress at the layer midpoint and subsequently assigned to the analysis. The initial shear modulus was determined using the following equation.

$$G_0 = A \cdot \sigma_m{}^n \tag{8}$$

Here, G_0 is the initial shear modulus, A and n are material-specific empirical parameters, and σ_m denotes the mean effective stress.

The stress-dependent parameter n was determined using the results of the bender element tests. The parameter A was derived for each analysis case using the least-squares method so as to minimize the discrepancy between the measured initial shear modulus obtained from shear-wave velocity and the estimated value computed from Eq. 8.

The boundary conditions for the seismic response analysis were defined by assigning a viscous boundary at the model base and energy-transmitting boundaries along the lateral sides. The dynamic deformation characteristics of the embankment and foundation soils were specified based on the dynamic properties of Inagi sand reported in ref. [16], those of cement-stabilized soil in ref. [17], and the Poisson's ratio values referenced from Tani et al. [10]. Table 1 summarizes the Duncan–Chang model parameters used in the initial stress analysis for, along with the parameters adopted in the seismic response analysis. Table 2 presents the parameters used in the plastic sliding analysis. The dynamic deformation characteristics of Inagi sand and cement-stabilized soil are shown in Fig. 3.

The analysis conditions were set to the normal full-reservoir water level, consistent with the centrifuge tests, and simulations were performed for both the upstream and downstream sides. In Level-2 seismic performance verification of road embankments, it is recommended that shallow surface sliding near the slope face be disregarded when defining the slip circle and that the slip arc be required to cross beneath the roadway, typically at a distance of approximately 4 m or more from the slope shoulder [18]. This study adopted a similar concept for dam embankments. To avoid superficial sliding and to ensure that the slip surface

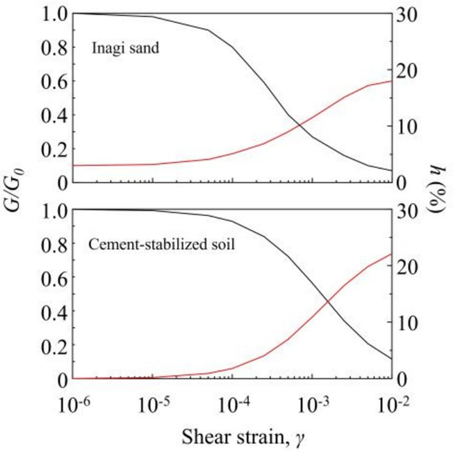

Fig. 3. Dynamic deformation characteristics of Inagi sand and cement-stabilized soil.

intersected the crest, two analytical cases were considered. One case applied a never-cut line (i.e., a constraint prohibiting slip surfaces from passing between the slope shoulder and toe) along both the upstream and downstream slopes, while the other applied no such restriction. In seismic performance verification of small earth dams subjected to Level-2 seismic motions, stability analyses are conducted to confirm whether the computed settlement remains within the prescribed allowable limits. By defining slip circles that cross the crest, the settlement associated with circular sliding of the embankment can be quantified, thereby enabling appropriate seismic performance evaluation under Level-2 seismic motions.

3 Results and discussion

3.1 Seismic response analysis

Fig. 4 presents the maximum shear strain distribution for each analysis case. In CASE 1, shear strain developed predominantly in the region slightly above the normal full-reservoir water level (H = 8.0 m) near the center of the embankment body. A pronounced concentration of shear strain occurred from the vicinity of the crest down

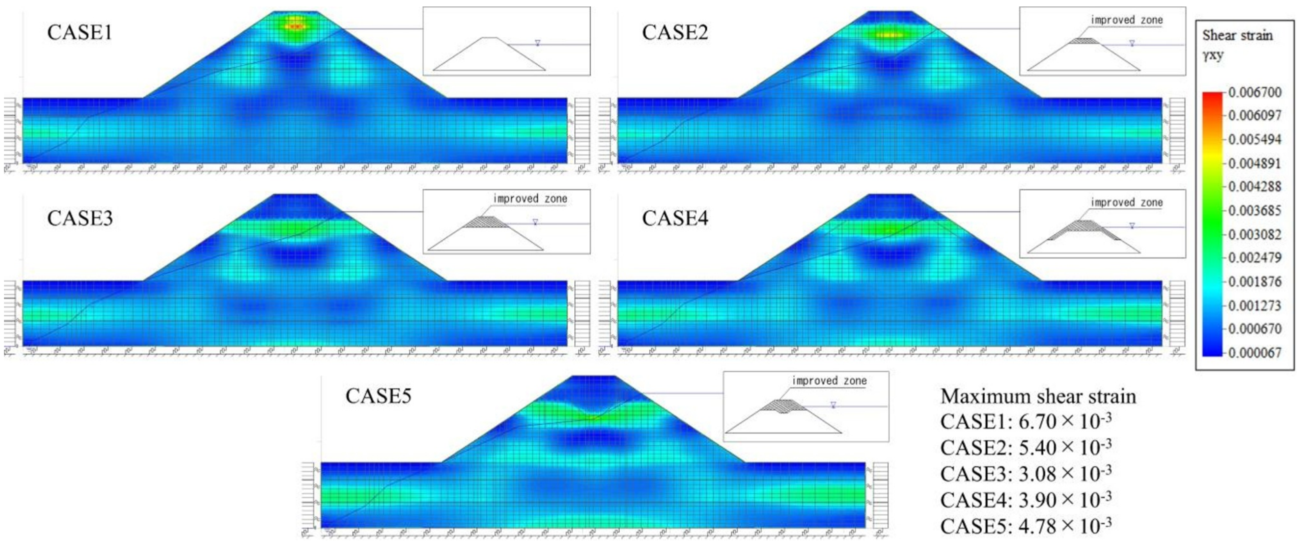

Fig. 4. Distribution of maximum shear strain for each experimental case.

to the unsaturated zone in the upper portion of the embankment, with a maximum value of 6.70×10^{-3}. In CASE 2, CASE 3, and CASE 5, the increase in shear strain within the improved zone was effectively suppressed. However, shear strain tended to concentrate near the interface between the improved and unimproved zones, in all cases where crest improvement was implemented, with maximum values of 5.40×10^{-3}, 3.08×10^{-3}, and 4.78×10^{-3}, respectively. A comparison of CASE 1 and CASE 2 indicates that crest-level solidification reduced the maximum shear strain in CASE 2. In CASE 3, where the improvement thickness was increased from 1.5 m to 3.0 m, the maximum shear strain was further reduced relative to both CASE 1 and CASE 2. These findings suggest that crest improvement is effective in suppressing the development of shear strain within the improved zone.

On the other hand, the observed concentration of shear strain at the boundary between the improved and unimproved zone indicates a potential for shear failure at this interface during seismic loading. This tendency is consistent with the observations reported by Tani et al. [10], who identified this boundary as a structural weak point. In addition, centrifuge tests conducted by Ohyama et al. [9] documented delamination at the same interface.

Furthermore, in CASE 4, outward deformation of the unimproved zone occurred during the 3.0 m/s² excitation stage, inducing tensile forces in the solidified toe portion of the improved zone and resulting in interface delamination.

3.2 Results of plastic slip analysis using the Newmark-D method

Table 3 summarizes the slip displacements on the upstream and downstream sides at the end of the analysis (t = 209.9 s) obtained using the Newmark-D method, along with the crown settlement measured after the 4.5 m/s² excitation stage in the centrifuge tests conducted by Ohyama et al. [9]. For CASE 4, the crest settlement could not be directly measured during the experiment; therefore, the settlement value presented in the table corresponds to the height difference near the center of the crest, as recorded by a laser displacement sensor before and after the centrifuge test [9].

Fig. 5 illustrates the maximum-displacement slip surface at the end of each analysis case (t = 209.9 s). It should be noted that the never-cut line used in some analyses is not shown in this figure. On the upstream side, the no-countermeasure case (CASE 1) exhibited slip displacement below the reservoir water level, with a maximum displacement of 1.78 m. In CASE 2, CASE 3, and CASE 5, the maximum-displacement arcs passed through the unimproved zone of the embankment without intersecting the improved zone. As summarized in Table 3 and shown in Fig. 5, the slip displacements for these cases were 4.33 m, 1.94 m, and 2.40 m, respectively, indicating substantial deformation. However, because the slip surfaces developed along the lower portion of the embankment slope and did not pass through the crest, the likelihood of direct crest settlement is low. Consequently, such slip behavior is unlikely to immediately trigger critical failure modes, such as rapid overtopping or uncontrolled release of reservoir water to the downstream side.

On the downstream side, the slip displacements were smaller than those observed upstream across all cases. This behavior is attributed to the broader distribution of the saturated zone on the upstream side, which promotes the accumulation of damage strain under seismic excitation and consequently leads to significant reductions in soil strength. The resulting degradation of shear strength is considered to be the primary factor contributing to the larger upstream slip displacements. In CASE 5, the downstream slip displacement reached 0.84 m, the largest among all cases. This relatively large displacement is likely attributable to the elevated seepage line compared with the other cases, as shown in Fig. 5, which would have enhanced the magnitude of strength reduction. In addition, the actual input acceleration waveform applied during the experiment was larger than initially assumed, as shown in Fig. 2, further contributing to the increased slip displacement.

Table 3. Sliding displacement calculated using Newmark-D method.

	Sliding displacement (m) (without never cut line)		Sliding displacement (m) (with never cut line)		Crest settlement of centrifuge experiment
	Upstream	Downstream	Upstream	Downstream	
CASE1	1.78	0.03	1.50	0.03	1.40
CASE2	4.33	0.01	1.23	0.01	0.98
CASE3	1.94	0.19	0.95	0.02	0.35
CASE4	2.45	0.24	1.68	0.24	1.68
CASE5	2.40	0.86	1.48	0.81	0.76

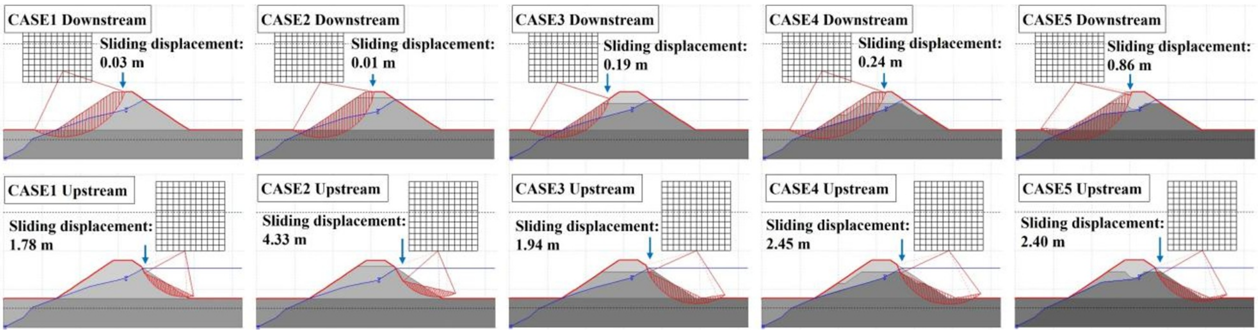

Fig. 5. Critical slip surfaces with the maximum displacement at the end of the analysis (t = 209.9 s) under the condition that no never cut line was applied along the slope.

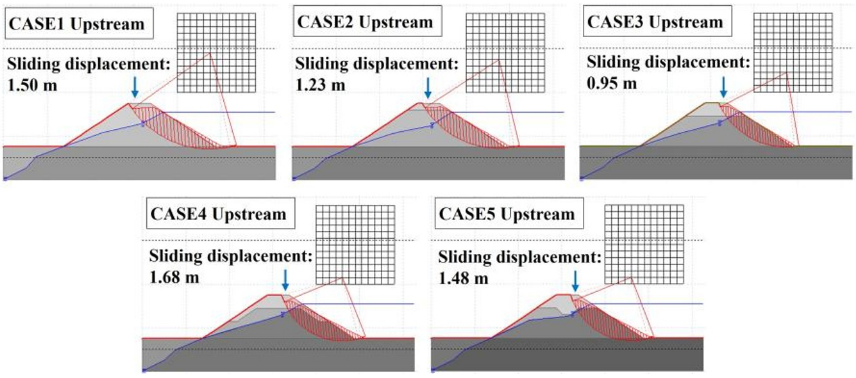

Fig. 6. Critical slip surfaces with the maximum displacement at the end of the analysis (t = 209.9 s) under the condition that a never cut line was applied along the slope.

Fig. 6 presents the maximum-displacement slip surfaces obtained for each analysis case at the end of the simulation under conditions where a never-cut line was imposed along the slope. Fig. 7 shows the average response acceleration, yield acceleration, and slip displacement (crest settlement) on the upstream side for CASE 1 through CASE 5, based on analyses in which the never-cut line was applied and the maximum-displacement arc was constrained to pass through the crest. As noted in Section 2.2, the Level-2 seismic verification method for road embankments recommends avoiding shallow surface sliding and selecting sliding arcs that cross the roadway [18]. This study applied the same concept to reservoir embankments. To ensure that the selected arc crosses the crest while excluding surface sliding, a never-cut line was set from the toe to the opposite toe. This constraint forces the maximum displacement arc to pass through the crest, allowing the resulting sliding displacement to be interpreted as crest settlement. It should be noted that, in the Newmark-D method, repeated undrained loading induces strength degradation within saturated zones. Therefore, the following discussion focuses on the upstream side, where the effects of strength reduction are most pronounced and the resulting settlement is the largest.

The maximum-displacement arc passing through the crest in CASE 1 resulted in a crest settlement of 1.50 m, as shown in Table 3 and Fig. 7. The corresponding crest settlements for CASE 2 and CASE 4 were 1.23 m and 1.68 m, respectively. The crest settlement values observed in the centrifuge tests for CASE 1, CASE 2, and CASE 4 were 1.40 m, 0.98 m, and 1.68 m, respectively, demonstrating good agreement with the settlement values obtained from the Newmark-D analysis. During the centrifuge tests, sliding occurred on the downstream side in CASE 1 and CASE 2 [9]. In CASE 4, tensile forces were induced during the 3.0 m/s² excitation stage, causing delamination of the solidified improvement zone and subsequent sliding. Although the sliding arc intersected a portion of the crest, the remaining freeboard indicates that this would not directly trigger a catastrophic event, such as immediate overtopping or uncontrolled downstream release of reservoir water.

In contrast, the crest settlements predicted using the Newmark-D method for CASE 3 and CASE 5 were 0.95 m and 1.48 m, respectively, whereas the

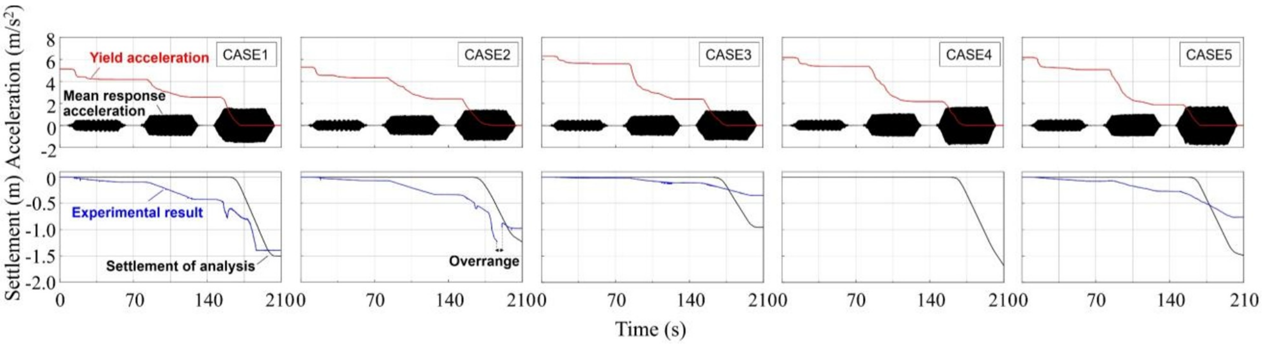

Fig. 7. Average response acceleration, yield acceleration, and slip displacement (crest settlement) on the upstream side.

corresponding crest settlements observed in the centrifuge tests were 0.35 m and 0.76 m. Thus, the settlement values obtained from the Newmark-D analysis were approximately twice those measured experimentally. Notably, in both CASE 3 and CASE 5, sliding accompanied by deformation did not occur during the centrifuge tests.

As shown in Fig. 7, the yield acceleration decreased progressively with increasing excitation stage for all cases from CASE 1 through CASE 5. However, no sliding occurred until the third excitation stage (4.5 m/s^2). Sliding displacements began to develop only when the vibration level reached 4.5 m/s^2. In CASE 1 and CASE 2, the crest settlement observed during the centrifuge tests at 4.5 m/s^2 exhibited trends similar to the slip displacements computed from the plastic sliding analysis.

3.3 Comparison of numerical analysis and centrifuge test results

In CASE1, CASE2, and CASE4—where sliding failure was the predominant deformation mode in the centrifuge loading tests—the crest settlements estimated using the Newmark-D method were generally consistent with the experimental values, falling within approximately 1.1 to 1.3 times the observed settlements. In contrast, CASE3 and CASE5 exhibited no distinct sliding during the centrifuge tests. Consequently, the applicability of the Newmark-D method—which inherently assumes sliding failure—was limited. The calculated crest settlements were approximately twice those observed in the centrifuge tests. These results indicate that when sliding displacement develops, the Newmark-D method can provide settlement estimates reasonably close to the experimental behavior. However, when sliding does not occur and rocking-type deformation dominates, the sliding displacement predicted by the Newmark-D method may exceed the measured crest settlement, yielding a conservative assessment.

The Newmark-D method assumes rigid-block motion along a predefined slip surface and presupposes the formation of a slip plane during seismic loading. Therefore, the method has inherent limitations when no sliding develops or when localized deformation mechanisms must be considered. Previous studies have noted that crest settlement in embankments during earthquakes may arise not only from sliding deformation but also from compressive deformation of embankment soils and settlement induced by cyclic shaking [19]. Okamura and Tamura [20] further identified shear deformation of the embankment, lateral spreading, and volumetric compression associated with soil liquefaction as important contributors to seismic deformation. When such non-sliding deformation modes dominate, the Newmark-D method may not adequately reproduce the deformation characteristics of the embankment. In situations where non-sliding deformation is expected to govern the seismic behavior, it becomes necessary to evaluate the dynamic response using dynamic effective stress analyses, such as LIQCA.

In this study, crest settlement was estimated by applying the verification procedure used for road embankments subjected to Level-2 seismic motion. To prevent surface sliding of the dam embankment, a never-cut line was introduced to constrain the slip arc so that it intersected the crest, and crest settlement was computed accordingly. However, when highly stiff elements such as cement-stabilized zones exist within the embankment, the arc corresponding to the maximum displacement may pass through the unimproved zone rather than the improved zone. Under the Level-2 seismic performance verification framework for small earth dams, compliance is determined by whether the calculated settlement is less than the allowable settlement specified in the guidelines [6]. However, if the analytical conditions are not appropriately defined, the arc of maximum displacement may not pass through the crest. As demonstrated in this study, this may lead to substantial sliding displacement occurring in unimproved zones near the embankment toe. Therefore, further examination is required to clarify the analytical conditions under which seismic performance verification should be conducted.

Moreover, in the cases analyzed in this study, sufficient freeboard remained even when sliding displacement occurred. Thus, such deformation would not immediately cause critical consequences, such as the rapid overtopping or uncontrolled downstream release of reservoir water. This indicates that, in addition to the allowable settlement criterion, engineering judgment regarding the preservation of reservoir-storage functionality—particularly whether adequate freeboard can be maintained—is essential when evaluating the seismic safety of dam embankments.

4 Conclusion

This study evaluated the seismic performance of dam embankments with improved crests subjected to Level-2 seismic motions and compared the analytical predictions with centrifuge test results. The findings showed that crest improvement suppressed the increase in shear strain within the improved zone, with the stabilizing effect becoming more pronounced as the improvement thickness increased. However, in all cases where crest improvement was applied, shear strain concentrations developed near the interface between the improved and unimproved zones, indicating the potential for shear failure or crack initiation.

When the maximum displacement arc passing through the crest was considered, the slip displacement calculated using the Newmark-D method showed generally good agreement with the settlement measured in the centrifuge tests for the cases without reinforcement, with 15% crest improvement, and with the Type-A improvement configuration. In contrast, for the case with 30% crest improvement and the convex-shaped improvement geometry, the slip displacement predicted using the Newmark-D method substantially exceeded the experimentally observed settlement. Although the Newmark-D method is based on the assumption that sliding occurs during seismic loading, no sliding developed in these centrifuge tests; instead, the dominant deformation mechanism was shaking-induced settlement. This mismatch between the analytical assumption (sliding) and the actual deformation mechanism (non-sliding) resulted in the observed discrepancies.

These results indicate that the Newmark-D method is appropriate when sliding displacement governs the embankment response. However, in cases where no sliding occurred and deformation was dominated by shaking-induced or localized strains, the method could not reproduce the observed behavior. In such situations, more advanced numerical approaches—such as dynamic response analysis or elastoplastic analysis—are required, as they can represent nonlinear soil behavior and localized deformation under strong ground motion.

This work was supported by JSPS KAKENHI Grant Number JP24H00533.

References

1. X. Liu, W. Liu, Q. Tang, B. Liu, Y. Wada, H. Yang, Global agricultural water scarcity assessment incorporating blue and green water availability under future climate change. Earth's Future. **10**(4), e2021EF002567 (2022). https://doi.org/10.1029/2021EF002567
2. Ministry of Agriculture, Forestry and Fisheries, Small earth dams. Accessed Jan. 5, 2026. Available from: https://www.maff.go.jp/j/nousin/bousai/bousai_saigai/b_tameike/index.html [in Japanese]
3. S. Tani, Damage to earth dams. Soils Found. **36**, 263–272 (1996). https://doi.org/10.3208/sandf.36.Special_263
4. S. Tani, Behavior of large fill dams during earthquake and earthquake damage. Soil Dyn. Earthq. Eng. **20**(1–4), 223–229 (2000). https://doi.org/10.1016/S0267-7261(00)00055-5
5. Y. Mohri, S. Masukawa, T. Hori, M. Ariyoshi, Damage to agricultural facilities. Soils Found. **54**(4), 588–607 (2014). https://doi.org/10.1016/j.sandf.2014.06.025
6. Ministry of Agriculture, Forestry and Fisheries, Japan (MAFF), Design guideline of land improvement project – small earth dam. MAFF, (2015). [in Japanese]
7. T. Momiyama, S. Taenaka, T. Hara, N. Tanaka, Study on reinforcement method of small earth dams using steel sheet piles: verification of reinforcement effect against the liquefaction through the shaking test. Trans. Jpn. Soc. Irrig. Drain. Rural Eng. **88**, I_47–I_58 (2020). https://doi.org/10.11408/jsidre.88.I_47 [in Japanese]
8. Y. Mohri, K. Matsushima, S. Yamazaki, T.N. Lohani, F. Tatsuoka, T. Tanaka, New direction for earth reinforcement: disaster prevention for earthfill dams. Geosynth. Int. **16**(4), 246–273 (2009). https://doi.org/10.1680/gein.2009.16.4.246
9. S. Ohyama, Y. Konishi, A. Izumi, H. Tagashira, Y. Sawada, Effect of crest improvement on the seismic stability of small earth dams. Soil Dyn. Earthq. Eng. **198**, 109622 (2025). https://doi.org/10.1016/j.soildyn.2025.109622
10. S. Tani, S. Tsukuni, T. Shiomi, Performance of a fill dam based on the performance-based design concept and study of a seismic retrofitting method. **49**(6), 841–851 (2009). https://doi.org/10.3208/sandf.49.841
11. Y. Huang, A. Yashima, K. Sawada, F. Zhang, Numerical assessment of the seismic response of an earth embankment on liquefiable soils. Bull. Eng. Geol. Environ. **67**, 31–39 (2008). https://doi.org/10.1007/s10064-007-0097-y
12. J. Jin, S. Lee, Liquefaction characteristics of aging earth dam body by dynamic centrifugal model test. Soil Dyn. Earthq. Eng. **181**, 108670 (2024). https://doi.org/10.1016/j.soildyn.2024.108670
13. A. Duttine, F. Tatsuoka, T. Shinbo, Y. Mohri, A new simplified seismic stability analysis taking into account degradation of soil undrained stress-strain properties and effects of compaction. In Validation of Dynamic Analyses of Dams and Their Equipment, CRC Press, pp. 215–234 (2018).
14. A. Duttine, F. Tatsuoka, K. Ueno, Effects of compaction on soil undrained shear strength deteriorating during undrained cyclic loading and controlling seismic stability of embankment. E3S Web Conf. **92**, 18003 (2019). https://doi.org/10.1051/e3sconf/20199218003
15. S. Yazaki, A. Duttine, Seismic stability evaluation of irrigation dams by the Newmark-D slip displacement analysis. Water. Land Environ. Eng. **92**(12), 879–883 (2024). [in Japanese]
16. Railway Technical Research Institute (RTRI), Design standards for railway structures and commentary (Seismic design). RTRI, (2012). [in Japanese]
17. National Institute for Land and Infrastructure Management, Ministry of Land, Infrastructure and Transport, Japan (NILIM), Technical note on seismic performance evaluation of dams against large earthquake. NILIM, (2005). [in Japanese]
18. Japan Road Association (JRA), Technical standards for road earthworks – Embankment construction. JRA, (2010). [in Japanese]

19. T. Hori, K. Ueno, K. Matsushima, Damages of small earth dams induced by the 2011 off the Pacific coast of Tohoku Earthquake. Tech. Rep. Natl. Inst. Rural. Eng. Japan, **213**, 175–199 (2012). [in Japanese]
20. M. Okamura, K. Tamura, Prediction method for liquefaction-induced settlement of embankment with remedial measure by deep mixing method. Soils Found. **44**(4), 53–65 (2004) https://doi.org/10.3208/sandf.44.4_53